Dynamical studies of fully oriented deuteropolyethylene by inelastic neutron scattering

J. F. Twisleton and J. W. White*
Physical Chemistry Laboratory, Oxford University, South Parks Road, Oxford OX1 3QZ, UK

and P. A. Reynolds
Department of Chemistry, University of Western Australia, Perth, Western Australia, Australia
(*Received* 29 *June* 1981)

Experimental parameters for interchain force fields of polyethylene are measured by neutron triple axis spectrometry and provide some of the first anisotropic information about the forces between carbon chains in simple polymers. Preparation of a bulk specimen of deuteropolyethylene with single crystal texture is reported for the first time. Near Brillouin-zone centre frequencies for both interchain optic and acoustic phonons are derived from neutron scattering studies. These measurements are combined with four frequencies obtained by Raman spectroscopy to give a total of seven experimental parameters for the interchain force field of polyethylene. These are then used to test the available force models. Overall fits of 9 and 19% are provided to these data by two Urey–Bradley force fields. Calculations of the interchain phonon dispersion curves of deuteropolyethylene based on an atom–atom potential parameter model are described. Intermolecular force constants which are derived from an analytical 'six-exp' form for the potential between nonbonded atoms are used. These reproduce a wide range of structural and thermodynamic data for many hydrocarbons. This rigid chain model using already fixed parameters fits the observed dynamical data within an average error of 5%. This is significantly better than the fits obtained using the Urey–Bradley force fields with adjustable parameters. The close reproduction of the experimental elastic constants gives support to the calculation of the related elastic moduli perpendicular to the chain axis. Tensile elastic moduli calculated along the two crystallographic axes perpendicular to the chain axis in the orthorhombic cell are very similar, in contrast with earlier predictions. The calculated values of 8×10^{10} and 9×10^{10} dyne cm^{-2} for *b* and *a* moduli agree closely with an average interchain modulus de4rived for the crystal from bulk measurements using a two phase 'sandwich' model of composite polyethylene.

Keywords Spectrometry; neutron scattering; inelastic; phonon dispersion curves; deuteropolyethylene

INTRODUCTION

Phonon dispersion curve measurements for polyethylene have long been restricted by the unavailability of specimens with a full single crystal texture. Feldkamp, Venkataraman and King[1] applied neutron triple axis spectrometry to a uniaxially oriented specimen of deuteropolyethylene (DPE) making direct observations of longitudinal acoustic (*LA*) chain skeletal vibrations throughout the Brillouin-zone. This work provided the first anisotropic information about the force field of polyethylene from neutron scattering. In a complementary work Twisleton and White[2] analysed coherent acoustic features in the neutron time-of-flight spectra of isotropic and uniaxially oriented DPE. Dynamical structure factor calculations illustrated the obvious contribution of *LA* phonons polarized along $[\zeta\,\zeta\,0]$ in the isotropically averaged phonon spectra. On the basis of these calculations an experimental elastic constant of the interchain force field was measured for the first time. In this present work the preparation of a bulk specimen of DPE with full single crystal texture is reported and neutron triple axis spectrometry is performed on this material. Measurements of the frequencies of acoustic phonons near the Brillouin-zone centre and of interchain optic phonons are reported. Analysis of the experimental data is assisted by dynamical structure factor calculations based on the 'atom–atom potential' model also described in this paper. The resulting experimental parameters are used in a criticism of this and other models for the interchain force field.

MODEL CALCULATIONS OF THE INTERCHAIN PHONON DISPERSION CURVES

Polyethylene is a composite material and one often refers to crystalline and amorphous phases within the bulk texture. In the 'crystalline regions' polyethylene chains stack in an orthorhombic lattice, with two chains in each unit cell. The crystal space group is D_{2h}^{16} or *Pnma*. Existing interchain force fields have been constructed by the definition of harmonic force constants between nearest-neighbour nonbonded hydrogen atoms[3–5]. These force constants are fitted to the rather meagre dynamical information pertaining to the interchain potential. This is mostly factor group splittings in Brillouin-zone centre optically active molecular deformational modes. Some

* To whom all correspondence is to be sent

0032-3861/82/040578-11$03.00

Table 1 Calculated and observed crystal structures of polyethylene

Structural parameter	Williams set IV calculated structure	Williams set VII calculated structure	Experimental structure 77K†
a (Å)	7.139	7.140	7.155
b (Å)	4.874	4.889	4.889
θ (degrees)	46.53	46.45	42.3
ϵ (kcal mol^{-1})	−1.465	−1.458	−1.838
Number of pairs	182	186	–
c (Å)	2.540	2.540	2.547
∡HCH (degrees)	104.0	106.0	106.0
∡CCC (degrees)	113.1	113.1	112.3
r_{C-H} (Å)	1.04	1.04	1.10
r_{C-C} (Å)	1.522	1.522	1.533

† Refs. 11, 12, 13

defects in these models have become apparent from earlier neutron scattering studies[2]. A more general approach to the formulation of an interchain potential employs nonbonded atom–atom pseudopotentials derived from structural and thermodynamic data for many hydrocarbons[6,7]. Such transferable parameters, using a six-exp analytical form for the potential between nonbonded atoms, have been produced by Williams[8,9]. The potential parameters reproduce well the crystal structure and heat of sublimation of polyethylene. These pseudopotentials are used here to calculate the equilibrium structure, a close approximation to the observed low temperature structure. Derivative properties of the potential are then calculated, at its minimum value, and from these the normal modes of external chain vibrations, their frequencies, amplitudes and other properties relevant to the neutron scattering studies reported here are estimated.

Structure calculations made here for polyethylene are valid within the limitations set by the methods used to obtain the potential constants themselves. For example, we used rigid molecules with an assumed geometry and the crystal space group was imposed from experiment, which implies coincidence of the crystallographic c-axis and chain axis. After this only three variables remained; the a and b lattice parameters and the setting angle θ between the chains. Minimization of the crystal potential with respect to these parameters proceeded by Powell's 'direct search' method[10] which defined the potential minimum with an accuracy of 0.01% in the structural variables. Summation limits of 5.0, 5.5 and 6.0 Å were employed for interactions between H–H, C–H and C–C nonbonded atom pairs respectively[8]. Since the number of pairs within these limits changed as the structural parameters were varied this number was fixed initially to avoid producing discontinuities in the potential function. Consequently exact reproduction of Williams' calculated structures[9] was not possible, although the results were very close to these. We used set IV (derived from aliphatic and aromatic hydrocarbon data), and set VII (aliphatic data only) since these embodied the most physically reasonable assumptions. *Table 1* summarizes the calculated structures obtained from Williams' set IV and VII potential parameters; the number of atom pairs considered; the sublimation energies ε; per CH_2 unit and the assumed intramolecular structural parameters. Comparison with the experimental structural and thermodynamic data[11–13] highlights the success of the atom–atom potentials which reproduce the observed lattice parameters within an error of at most 0.2%. For the setting angle θ, the angle between the plane containing the C–C bonds of a chain and the crystal bc plane, agreement is poorer although there is still much controversy about the experimental value. Smith[14] quotes 48° from his analysis of X-ray diffraction data from the n-paraffins and Shearer and Vand[15] quote 48.6° for monoclinic $C_{26}H_{74}$. In contrast Bunn[16] reports a figure of 41.3° and the value of Teare[12] given in *Table 1* is 42.3°. Further experimental work is clearly required. For the moment it is very hard to dispute the calculated values which lie around 46.5°. The calculated sublimation energy is low due to the distance truncation in the summation. This truncation affects the structure and dynamics far less.

Phonon dispersion curves for interchain vibrations in polyethylene were calculated from the analytical potentials using the computer program CRISS–CROSS kindly provided by Dr G. S. Pawley. This program[17,18] was originally designed for calculating external lattice vibrational frequencies of rigid centrosymmetric molecules in crystals with two molecules in the unit cell and as such was ideally applicable to polyethylene. In CRISS–CROSS intermolecular force constants were derived by functional differentiation of the crystal potential at its minimum value, i.e. with the structural parameters defined in *Table 1*. The dynamical matrix (equation (5) in ref. 17) was then constructed and solved to give phonon frequencies and molecular amplitudes in the normal modes.

Polyethylene is effectively a two dimensional molecular crystal since one of the crystallographic axes coincides with the axis of an extended molecular chain. Consequently the four 'external' normal modes involving librations about the a and b axes are in fact intrachain deformations, reducing the number of genuine external chain modes to eight. Such internal chain stretching and bending modes have been observed around 1000 cm^{-1} by Raman and infra-red techniques and are essentially decoupled from the lower frequency interchain vibrations. In the external mode calculation using CRISS–CROSS, the chain is treated as being discontinuous at the cell boundaries with the underlying assumption that dynamical properties derived for a single C_2H_4 unit pertain to the extended chain. This means that the force constants are scaled by the same factor as the mass and inertia terms, as the chain segment length is increased, so that dynamical matrix elements remain constant. This assumption was corroborated by a series of calculations for $C_{2i}H_{4i}$ segments up to $C_{20}H_{40}$, all of which yielded the same phonon frequencies and molecular eigenvectors. In these calculations the inertial axes for $C_{2i}H_{4i}$ segments were redefined to take account of their incorporation within an infinite chain. In CRISS–CROSS this was achieved by introducing two dummy atoms of very large mass at displacements above and below each segment upon the crystallographic c-axis so that the principal axes of inertia became defined along and perpendicular to this axis. Moreover, dynamical matrix elements for the librations forbidden on a rigid chain model disappeared then since the inertial denominators in equation (5) of ref. 17 became very large for rotations about the a and b axes. In this limit the dynamical matrix requiring solution reduced in dimensions from 12×12 to 8×8.

Symmetry points and lines in the Brillouin zone of

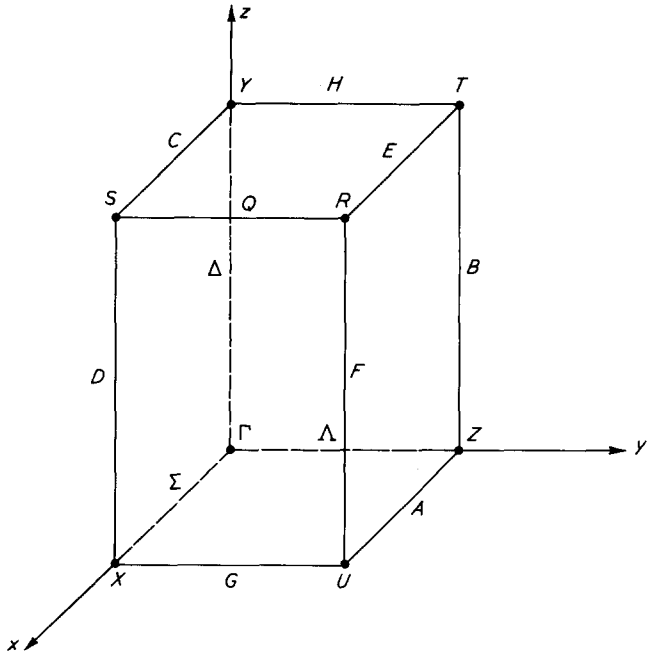

Figure 1 Symmetry points and lines in the Brillouin-zone of orthorhombic polyethylene labelled after ref. 19

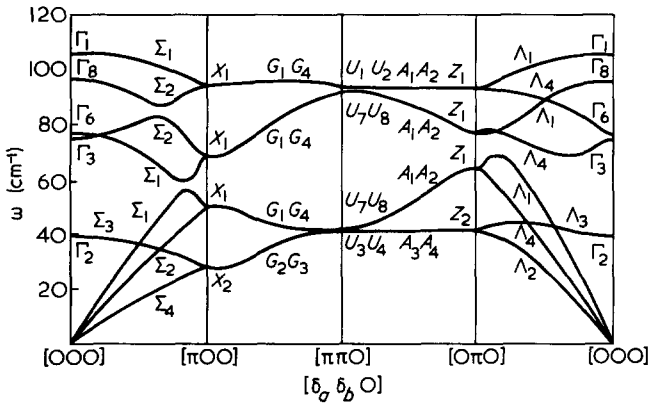

Figure 2 Interchain phonon dispersion curves for DPE calculated for rigid molecules using Williams set VII potential parameters

orthorhombic polyethylene are labelled in *Figure 1* using the nomenclature of Slater[19]. Crystallographic *a*, *b* and *c* axes correspond here to the *x*, *y* and *z* polarizations. Kitagawa and Miyazawa[20] have tabulated representations for groups of the phonon wave vector $\vec{q}$ which greatly facilitates the symmetry classification of normal modes of external vibrations in polyethylene. Phonon dispersion curves for interchain vibrations in DPE calculated using the set VII six-exp potential parameters of Williams are shown in *Figure 2* as a function of $[\delta_a \delta_b 0]$ where

$$\delta_a = a q_a \quad \delta_b = b q_b \quad \delta_c = c q_c \qquad (1)$$

As presented the solutions are for $\vec{q}$ values along the zone edges defined by the symmetry lines Σ, *G*, *A* and Λ described in *Figure 1*, with $\vec{q}$ restricted to the basal plane of the polymer. Normal mode symmetries were derived from the transformation properties of the eigenvectors in the local $\vec{q}$ group and the irreducible representations are labelled after ref. 20. At the zone centre Γ(000) point the $\vec{q}$ group attains its highest symmetry of D_{2h}, the factor group of the crystal space group D_{2h}^{16}. Five external modes have non-zero intercepts at the zone centre and *Figure 3* represents the eigenvectors for each mode, making clear the distinction between translatory and rotatory modes. Of these modes two are infra-red active, Γ_6 and Γ_8, corresponding to antiparallel translation of the chains in the *b* and *a* directions with B_{1u} and B_{2u} symmetry respectively. Another two modes, Γ_1 and Γ_3, correspond to external librations about the *c*-axis with A_g and B_{3g} symmetry and both are Raman active. The remaining $\Gamma_2(A_u)$ vibrations are inactive in both the infra-red and Raman spectra and involve antiparallel motion of the two chains in the unit cell along the *c*-axis. On moving away from the zone centre $\vec{q}$ group symmetry is reduced from D_{2h} to C_s in all but the $[\zeta\,0\,0]$ and $[0\,\zeta\,0]$ directions for which C_{2v} symmetry is preserved. Along $\Sigma[\delta\,0\,0]$ and $\Lambda[0\,\delta\,0]$ there are four representations, two of which attach to antiparallel translations of the chains along the *c*-direction and cross over the remaining *ab* polarized modes. Since the remaining six modes belong to one of two irreducible representations of the C_{2v} $\vec{q}$ group they mix extensively as *Figure 2* illustrates. The degeneracies at $[\pi\,0\,0]$ and $[0\,\pi\,0]$ persist around the zone edges and are attributed to a time reversal degeneracy, discussed by Kitagawa and Miyazawa[20].

Comparison of these results with experiment and the earlier calculations is made after the experimental section. It should be noted here that the set IV and VII potentials of Williams yielded lattice frequencies in very close agreement (see *Table 4*) as might be expected from their nearly identical reproduction of the crystal structure.

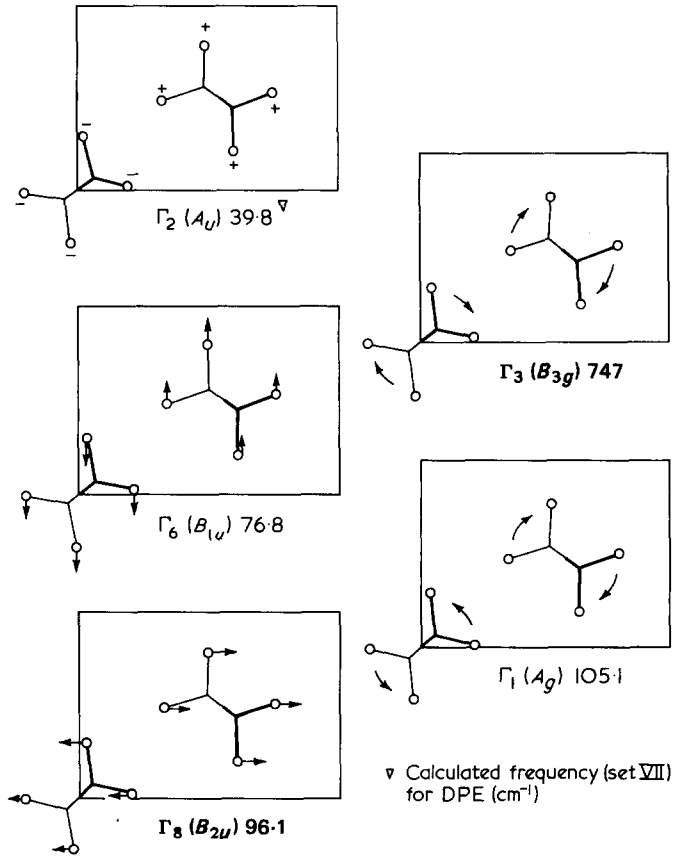

Figure 3 Explicit representation of the eigenvectors for normal modes at the zone centre Γ point of orthorhombic polyethylene

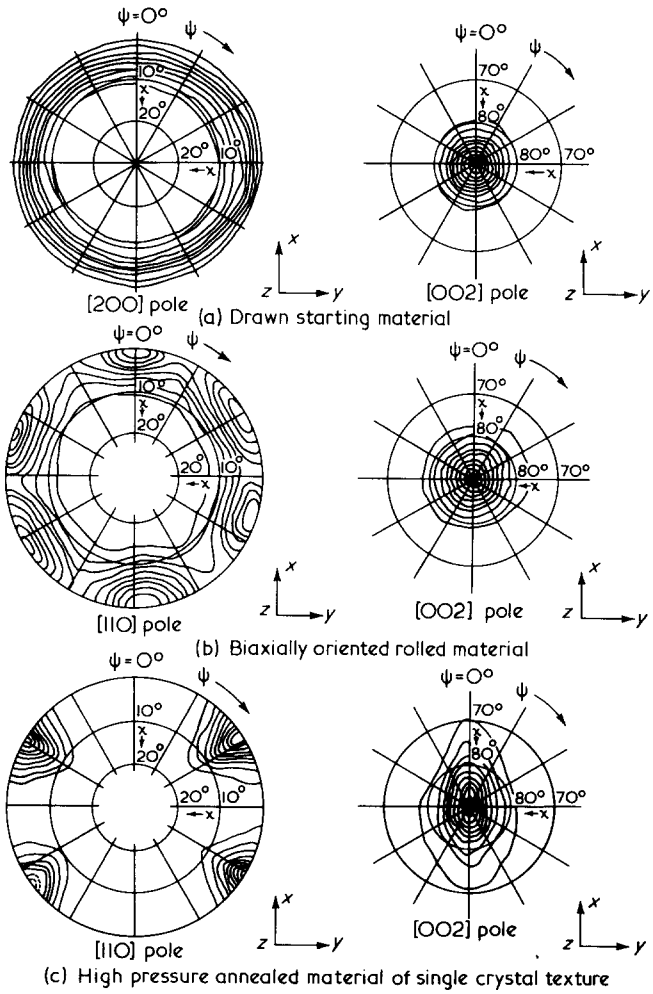

Figure 4 Pole figures for drawn, rolled and annealed DPE showing the development of orientation along and perpendicular to the chain direction

PREPARATION AND CHARACTERIZATION OF SINGLE CRYSTAL TEXTURED DEUTEROPOLYETHYLENE

On account of the composite nature of polyethylene the preparation of samples in which the crystallites achieve a common orientation is difficult. Uniaxial orientation of the chains in the c direction in the crystalline regions is readily obtained by stretching the isotropic melt crystallized polyethylene[2,6]. Moreover, some three dimensional ordering is introduced on the application of biaxial stress by rolling or extruding the isotropic material. Here the c-axes orient in the direction of maximum tensile stress with the a and b poles attaining a twinned configuration in the basal plane of the polymer. Removal of this twinning was first reported by Hay and Keller[21] who annealed biaxially oriented polyethylene obtaining a single crystal texture. Some loss of c-orientation on annealing was associated with a contraction in specimen length and this was remedied by Bowden and Young[22,23] who devised a high pressure annealing process with a constraint on the specimen shape. This process was investigated by the present authors with a view to reducing the mosaic spread in the basal plane of the product by careful choice of pressure and annealing temperature. Specimens of DPE with single crystal texture were then prepared and used in triple axis neutron spectrometry.

Stretch oriented DPE was provided by Dr J. S. King, Nuclear Engineering Dept., University of Michigan. This sample was employed by Feldkamp, Venkataraman and King in their measurements of acoustic chain phonons[1]. Pole figures obtained using a Hilger Watts automatic four-circle diffractometer[24] are shown in *Figure 4a* for this material. In *Figure 4* intensity contours represent percentages of the maximum intensity of a given reflexion. Polar angles χ and ψ are defined in the sample framework where Z indicates the draw direction and X the direction normal to the plane of the specimen. Projections of the spherical distribution of reflexion planes onto a flat surface are presented for convenience and since the c-orientation is so good projections from the χ circle are restricted to a 20° arc to avoid grouping the contours too closely. Contours are plotted from 10% to 90% of the maximum intensity and a good estimate of the mosaic F.W.H.M. is obtained from the dimensions of the 50% contour. In the drawn starting material $[h\,k\,0]$ planes show no preferred orientation perpendicular to the chain axis rather giving rise to a series of concentric rings on the pole figure as shown in *Figure 4a* for [200]. By contrast the [002] poles are aligned about the Z-axis within 8° F.W.H.M.

Sample treatment was in two stages each of which contributed to the final orientation. Rolling of the drawn material with the direction of advance in the draw direction induced some orientation in the basal plane. Specimen thicknesses were reduced from 0.017″ to 0.012″, a reduction of 30%. Further rolling caused crazing and general deterioration of the sample. Pole figures for the rolled material are shown in *Figure 4b*. There is a slight relaxation in c-orientation while a six point pattern emerges for $[h\,k\,0]$ reflexions, which arises from twinning of the single crystal texture. Each set of $[h\,k\,0]$ planes has a twin at $\pm 60°$ to the original direction[21].

Twinning in the basal plane was removed by annealing under pressure. A series of 1″ diameter discs was cut out of the rolled material and inserted in pairs within a circular pyrophyllite clay washer illustrated in *Figure 5*. Pressure

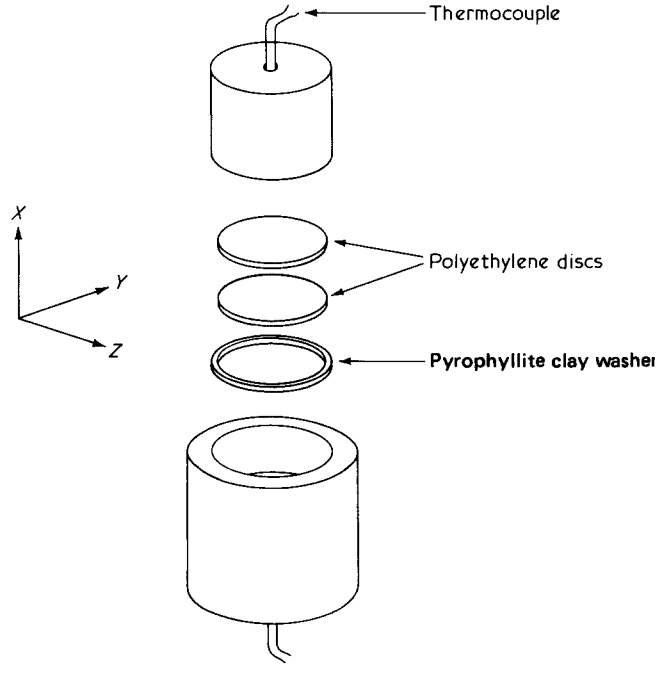

Figure 5 High pressure annealing assembly

was applied and the assembly heated to a temperature near to the melting point at that pressure. After annealing the platen assembly was cooled by water injection with the pressure maintained and the oriented specimens recovered. Temperature, pressure and annealing time were systematically varied to optimize the mosaic spread of *a* and *b* poles in the product, characterized initially by flat plate X-ray photographs[6]. A load of 11 tons was finally chosen, corresponding to a sample pressure of 2.1 kbar. Annealing at 185±3°C for 15 min gave the best results. At this pressure the melting point was 190±3°C which is in good agreement with the value of 191°C found by Baer and Kardos[25] for hydrogenous polyethylene (NPE), implying that the pressure on the sample had been correctly estimated from the load and disc area. Pole figures for the annealed product are illustrated in *Figure 4c* and show the single crystal texture and removal of twinning in the basal plane. The four '[110]' reflexions appear and [200] and [020] align along *X* and *Y* respectively with mosaic as low as 14° F.W.H.M. perpendicular to the draw direction. There is some relaxation of the *c*-mosaic in the *XZ* plane on annealing giving an average F.W.H.M. of 10° compared to an initial 8° F.W.H.M.

Choice of annealed discs to assemble into the final specimen for neutron triple axis spectrometry was affected by two factors: mosaic in the basal plane and the intensity of Bragg reflexions in a particular sample compared with the level of background scattering. Density measurements indicated that specimens contained at least 25% of amorphous material which was partially responsible for the observed backgrounds. Variations in the ratio of peak background intensity from disc to disc could not be explained solely by changes in amorphous content. It became clear that a fraction of the crystallites were still randomly oriented in some of the discs which must be seen as composites of 'single crystal', 'polycrystal' and 'amorphous' textures. Discs were selected on the basis of their mosaic and 'single crystal' content, stacked in an aluminium frame, and then manually aligned using a neutron diffractometer. The resulting sample contained 0.48 g of DPE and possessed a mosaic of 17° F.W.H.M. in the basal plane of the polymer. In appearance the discs were yellowish to light brown, although comparison with the starting material showed that very little additional degradation had occurred on annealing. Lattice parameters at 77K derived from the neutron diffraction data were in excellent agreement with earlier measurements summarized in *Table 1*.

TRIPLE AXIS NEUTRON SPECTROMETRY OF SINGLE CRYSTAL TEXTURED DEUTEROPOLYETHYLENE

Neutron inelastic scattering studies of single crystal textured DPE were restricted to the basal plane of the polymer and employed the TAS II triple axis spectrometer at A.E.K. Risø[6]. Pyrolytic graphite was employed in the monochromator and analyser systems. This gave a large enough count rate from the small specimen due to both the high reflectivity of graphite and from the choice of crystals with appreciable mosaic, 0.5 and 1.2° respectively[26]. Incident neutrons were reflected off the [002] planes and second order contamination was removed by a graphite filter giving an essentially monochromatic beam of wavelength 2.40 Å. Further enhancement of the count rate was achieved by relaxing the collimation within limits determined by the associated deterioration in energy resolution. In this way a count rate of 30 c.p.m. above background was achieved for the best phonon group. Experimental phonon groups were observed by the method of 'constant $\vec{Q}$' and it is convenient to treat the results under two headings.

Acoustic phonon measurements

Longitudinal and transverse scans for interchain acoustic phonon groups were performed in the vicinity of Bragg points in the basal plane, i.e. [220], [200], [020], [120] and [310]. Only low $\vec{Q}$ Bragg reflexions were studied to minimize the effects of the mosaic spread. After a series of scans about these Bragg points it was concluded the *LA* phonons could be measured only in the vicinity of [220], [200] and [020]. Scans for transverse phonons were frustrated by the wide mosaic. Typical constant $\vec{Q}$ scans with neutron energy loss are shown in *Figure 6* for the [ζ00] polarization. The energy range of phonon measurements was restricted at low energies (<15 cm^{-1}) by the presence of the resolution broadened elastic peak and at high energies (>40 cm^{-1}) by the lower intensity and greater width of phonon groups well away from the Brillouin-zone centre.

Much attention was given to the problem of extracting the phonon groups from the background, which came mainly from incoherent elastic scattering. Various analytical forms were employed to describe both the phonon group and the residual scattering in attempts at a

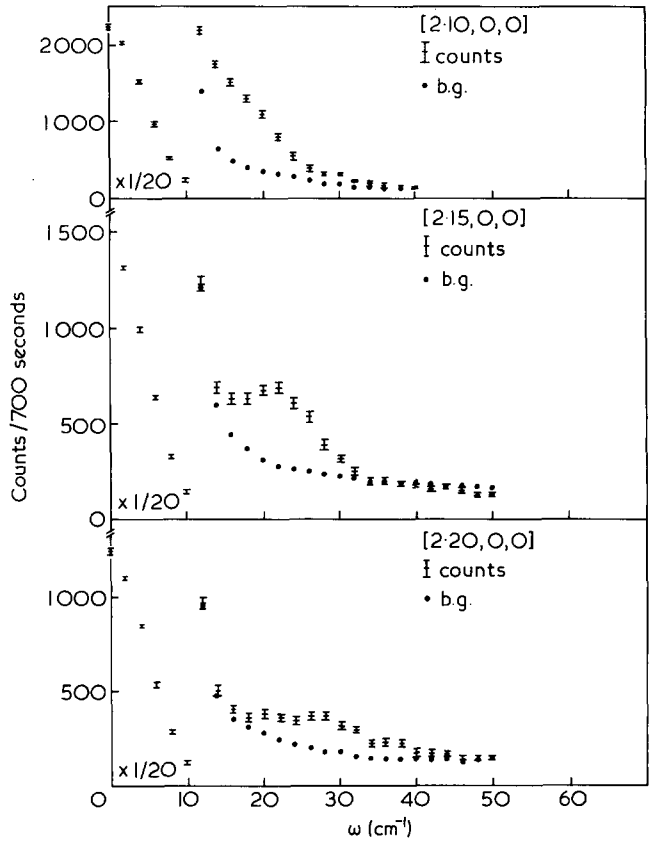

Figure 6 Neutron energy loss spectra at constant $\vec{Q}$ sites along [ζ00] for single crystal texture DPE at 77K

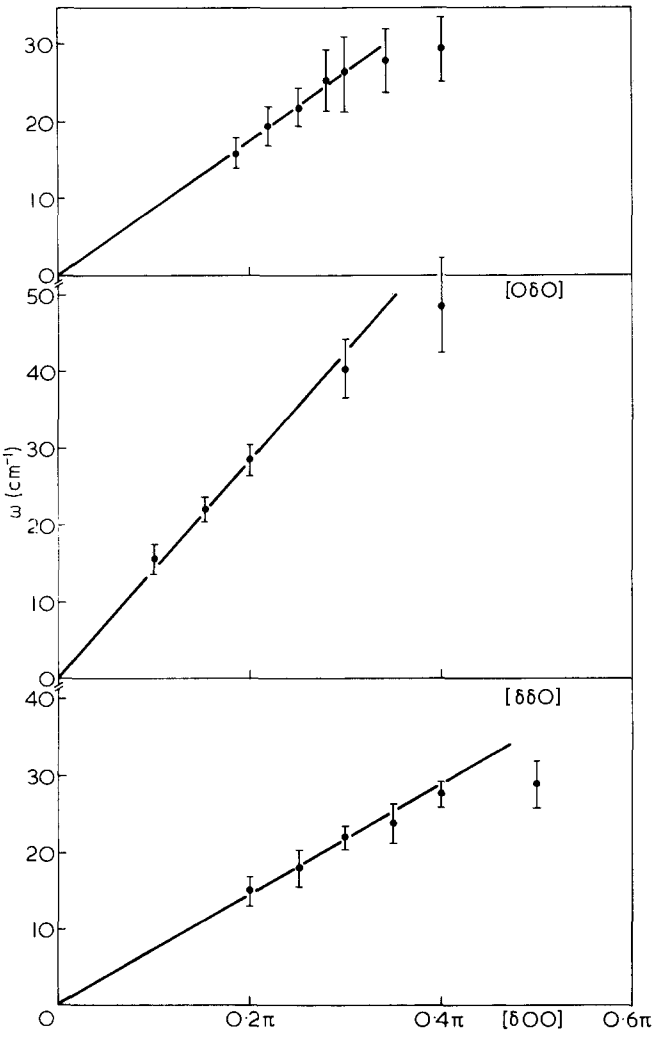

Figure 7 Experimental phonon groups parametrized by the phase angle $[\delta_a \delta_b 0]$ derived from the geometry of the co linear configuration of $\vec{Q}$, $\vec{q}$ and $2\pi\vec{\tau}$ in *Figure 8a*

deconvolution of the two contributions by fitting to the total energy spectrum[6]. This procedure failed because a satisfactory analytical description of the mosaic broadened groups and the background required too many variables, so that the experimental data were insufficient to define these functional parameters in a unique sense. In particular, a simple description of the elastic scattering in terms of Gaussian contribution was inadequate. There was an additional non-Gaussian component in the scattering, revealed by examining constant $\vec{Q}$ scans at Q values well away from the zone centre, which minimizes the phonon contribution. An alternative method of subtracting the background was adopted. It was assumed that the shape of the background, after subtracting a constant-in-energy linear-in-time background, was constant for a series of constant $\vec{Q}$ scans, collinear in reciprocal space. In this approximation the background counts were constructed from the renormalized energy spectrum, which was taken at a point so distant from the reciprocal lattice point that the phonon contribution had disappeared. Backgrounds calculated in this way are reproduced in *Figure 6*.

Experimental phonon groups located in this manner are assembled in *Figure 7* as plots of phonon frequency against phase angle (1) along the [0ζ0], [ζζ0] and [ζ00] directions. The calculations proved to be a valuable guide for explaining many unusual features in the neutron spectra such as the marked broadening of the observed groups across the zone. This is reflected by the increased amplitude of the error bars in *Figure 7*. In the case of the [0ζ0] data this broadening suggests that the phonon group is splitting into two peaks, though the poor statistics in the region of interest make this uncertain. The [ζ00] data show a sudden departure from a linear dispersion relationship around the half zone mark. This suggests the emergence of an additional contribution to the scattering, secondary to the *LA* component of the experimental phonon group, and at lower frequency.

Calculations of the mosaic broadening of phonon excitations based on the potential parameter model give an interpretation of these effects. The total coherent inelastic cross section[6] for phonon excitations in a constant $\vec{Q}$ scan must be written as a sum over the various configurations of $\vec{q}$, $\vec{Q}$ and the reciprocal lattice vectors $2\pi\vec{\tau}$ generated by the mosaic and parametrized by the angle θ in *Figure 8a*. Once configurations of $\vec{q}, \vec{Q}$ and $2\pi\vec{\tau}$ derived from the mosaic spread in the basal plane were considered because eigen-solutions from the rigid chain model were the only ones available.

This is only a first approximation since the spread about the c axis is at least half that in the basal plane. The total cross section then becomes, for neutrons losing energy

$$\frac{d^2\sigma}{d\Omega dE_{coh}} = (2\pi)^3 \sum_{j\theta} \frac{k}{k_0} \delta(\hbar\omega - \hbar\omega_j(\vec{q}))_\theta F_j(\theta) \qquad (2)$$

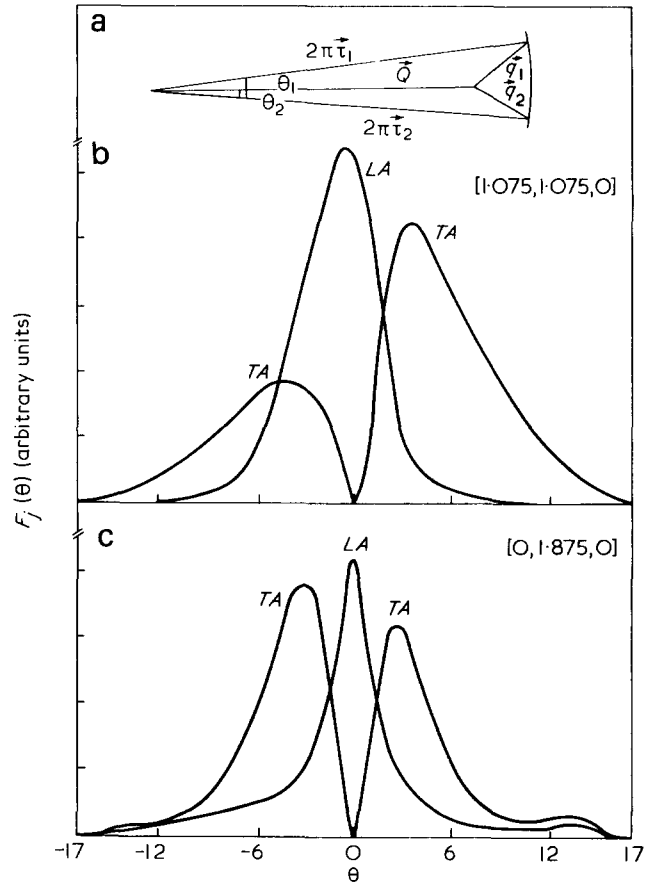

Figure 8 (a) Scattering diagram illustrating the range of $\vec{q}$ vectors generated at constant $\vec{Q}$ by the mosaic spread of $2\pi\vec{\tau}$. (b) Polar variation of $F_j(\theta)$ for *LA* and *TA* modes excited at [1.075, 1.075, 0]. (c) Polar variation of $F_j(\theta)$ for *LA* and *TA* modes excited at [0, 1.875, 0]

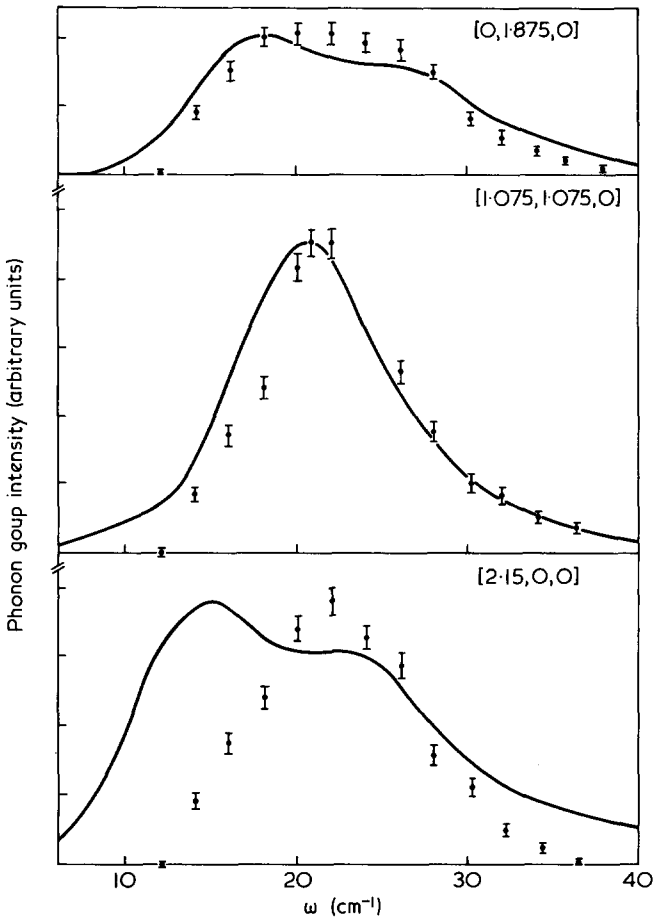

Figure 9 Calculated (——) and observed (●) phonon groups for DPE with basal plane mosaic 17° F.W.H.M.

where

$$F_j(\theta) = G(\theta)|g_j(\vec{Q})|^2(n_{\vec{q}j}+1)\delta(\vec{Q}+\vec{q}-2\pi\vec{t})_\theta \qquad (3)$$

and

$$g_j(\vec{Q}) = \sum_v (\hbar/2M_v\omega)^{1/2} b_v.(Q.\vec{\zeta}_{vj}(\vec{q})).(e^{-W_v\vec{Q}.\vec{\alpha}_v}) \qquad (4)$$

is the familiar dynamical structure factor[27]. In equation (4) the summation runs over atomic positions $\vec{\alpha}_v$, masses M_v, scattering lengths b_v, amplitudes $\vec{\zeta}_{vj}(\vec{q})$ and Debye Waller factors W_v with the subscript j covering the normal modes of the crystal. The phonon population $n_{\vec{q}j}$ is given by the Bose factor $(e^{\hbar\omega_j(\vec{q})/kT}-1)^{-1}$ and $G(\theta)$ is a triangular approximation to a Gaussian function of F.W.H.M. equal to the mosaic spread in the basal plane. $G(\theta)$ weights the dynamical structure factors of the excitations illustrated in *Figure 8a* as a function of θ taking into account the Gaussian distribution of poles about the nominal point in the scattering plane.

Calculations were performed using the eigensolutions $\omega_j(\vec{q})$ and $\vec{\zeta}_{vj}(\vec{q})$ from the rigid chain potential parameter model, simulating constant $\vec{Q}$ scans along [ζ00], [ζζ0] and [0ζ0]. Although *LA* modes excited in the parallel configuration of the three vectors in *Figure 8a* were the most distinct excitations, the $\vec{q}$ components inclined to $\vec{Q}$ and terminating the arc defined by the range of lattice vectors in some cases also contributed to singularities. Such contributions arose from nominal transverse acoustic (*TA*) modes propagating in the basal plane and of lower frequency than the *LA* modes. In *Figures 8b* and *8c* the functions $F_j(\theta)$ for *LA* and *TA* modes excited in longitudinal scans near [110] and [200] Bragg points are shown for the series of $\vec{q}$ values parametrized by the mosaic angle θ. The relative importance of *LA* and *TA* phonon contributions can be assessed from the areas enclosed in the figures.

Frequency distributions derived by summing $F_j(\theta)$ for all θ and j, folding the resulting histogram with the resolution function and multiplying by an arbitrary constant are shown in *Figure 9* together with the observed groups for comparison. These calculations partially succeed in reproducing the [0ζ0] and [ζζ0] experimental groups. The large widths of [0ζ0] groups are then explicable since the calculations predict that [ζζ0] *TA* and [0ζ0] *LA* phonons contribute to the total cross section with about equal weight to give broad doublets, suggested to some extent by the experimental data[6]. Again the [ζζ0] data are very closely reproduced by the calculations which confirm that the *LA* component predominates in the total cross section. For the [ζ00] data there is a serious discrepancy between the observed peak and the calculated profile, which is much broader and shifted to lower frequency. The balance between *TA* and *LA* components is very delicate along [ζ00] with the calculated width a sensitive function of $\vec{q}$ as the dominant contribution changes from the higher energy (*LA*) to the lower energy (*TA*) mode. From the discrepancy between calculation and experiment it would appear that the calculations fail to predict the point along [ζ00] at which the *TA* mode begins to contribute significantly.

Experimental widths for the [ζ00], [ζζ0] and [0ζ0] groups are plotted as a function of energy in *Figure 10*. The widths seem to fall into two categories, the narrower type most likely attributable to pure *LA* excitations while the broader group pertain to mixed *LA–TA* excitations. In the case of [ζ00] groups the widths increase gradually up to [2.25,0,0] where there is a sudden jump from 14 to 20 cm^{-1}. This discontinuity is reflected in *Figure 7* by a sharp departure from the linear dispersion relationship at

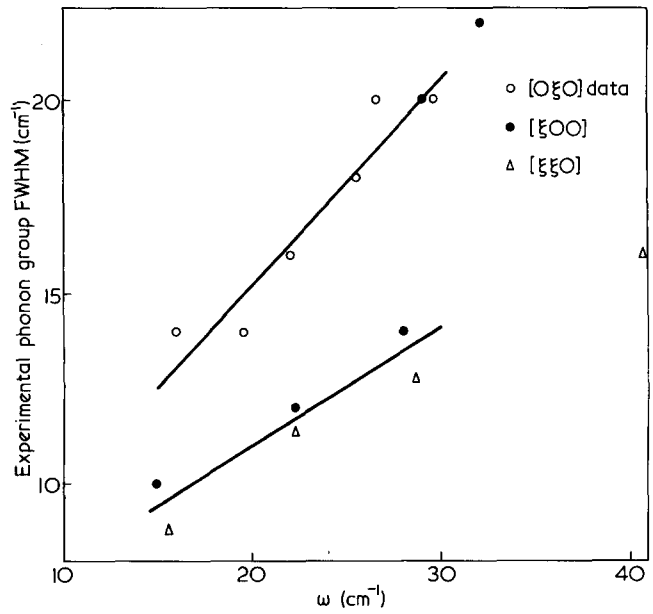

Figure 10 Experimental phonon group widths assembled as a function of their energy for [ξ00], [ξξ0] and [0ξ0] groups

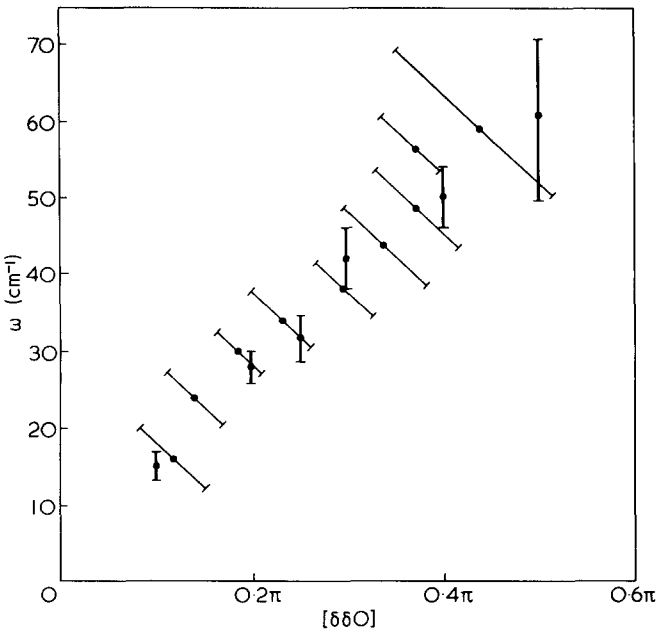

Figure 11 Experimental *LA* phonon groups along [ζζ0] from time-of-flight experiments (●) on *c*-oriented DPE compared with those derived from triple axis constant $\vec{Q}$ scans (●) on single crystal texture DPE, both at 298K

Table 2 Calculated dynamical structure factors for zone centre scans at [*hk*0] in DPE

Mode	$\omega^{\dagger}$ (cm^{-1})	$\lvert g_j(\vec{Q})\rvert^2 (n_{0j}+1)$ [010]	[300]	[120]
B_{3g}	74.7	183	1947	310
B_{1u}	76.8	1308	0	25
B_{2u}	96.1	0	474	2
A_g	105.1	0	0	2488

† Calculated Williams set VII

[2.25,0,0]. On this basis it is reasonable to postulate that the [ζ00] groups retain their *LA* character up to this point and thereafter become a synthesis of *TA* and *LA* modes with a consequent downward shift in the peak centre frequency and increase in peak width.

There are thus three acoustic slopes definable from the experimental data at 77K. Two of these can be related to single branches of the interchain dispersion curves although the third must be seen as a combination of two branches in about equal proportions. Elastic constants of 11.5×10^{10} and 14.2×10^{10} dyne cm^{-2} were determined from the calculated slopes along the [ζ00] and [ζζ0] directions at 77K, with an error of 6% representing a 3% estimated error in the acoustic slope determination. An elastic constant of 6.5×10^{10} dyne cm^{-2} was derived from the [0ζ0] data with the assumption that the observed ponons represented an exact mean of the [0ζ0] *LA* and [ζζ0] *TA* branches employed in defining a mean phonon wave vector.

Finally experimental data at room temperature for [ζζ0] *LA* phonons are reproduced in *Figure 11* together with the singularities obtained in earlier time-of-flight studies of uniaxially oriented DPE. As can be seen the two sets of data are in good agreement, defining moduli of $(13.5 \pm 0.8) \times 10^{10}$ and $(15 \pm 3) \times 10^{10}$ dyne cm^{-2} respectively at 298K. This lends support to the arguments used in ref. 2 for the assignment of the singularities observed in polycrystalline and uniaxially oriented DPE.

Zone centre mode investigation

Constant $\vec{Q}$ scans at reciprocal lattice points were used to obtain some zone centre external modes. Choice of lattice point was assisted by dynamical structure factor calculations which are summarized in *Table 2*. Only three of the five modes in *Figure 3* could be investigated since the region of $\vec{Q}$ space experimentally accessible was restricted, on the low $\vec{Q}$ side by contamination of the scattered counts by the straight-through beam, and on the high $\vec{Q}$ side by the increasing significance of sample mosaic. Consequently although the B_{2u} mode was calculated to appear in strength only at [100] this lattice point was inaccessible for the first reason. Zone centre constant $\vec{Q}$ scans taken at [120] and [010] with neutron energy gain are illustrated in *Figure 12* where lines have been drawn in to underline statistically significant singularities. The sharp rise in intensity above 90 cm^{-1} in the [010] scan is attributable to a contribution from unscattered neutrons which increases as the counter approaches the straight-through beam position. Unfortunately, there is no easily justifiable method for constructing backgrounds to these scans. Two singularities are evident in the data exhibited. They lie at 72 ± 3 and 111 ± 3 cm^{-1} in the [010] and the [120] scans respectively. A weak feature at 96 ± 5 cm^{-1} has also been observed in a scan taken at the [300] lattice point.

According to the calculated structure factors of *Table 1* prominent features are expected from B_{1u}, A_g and B_{3g} modes in the [010], [120] and [300] scans respectively. It is reasonable to assign the 72 and 111 cm^{-1} peaks on the basis of the calculations since there appears to be only one strong feature in both calculated and experimental scans. Moreover the *b*-translating B_{1u} mode has been observed in NPE already by far infra-red spectroscopy[28] and so a

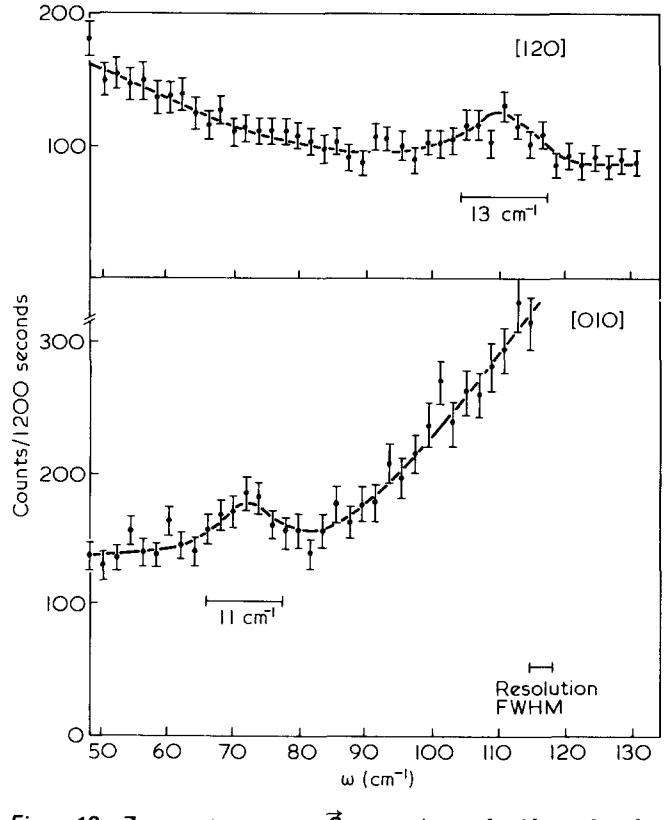

Figure 12 Zone centre constant $\vec{Q}$ scans taken at [120] and [010] with neutron energy gain from DPE at 77K

Table 3 Calculated and experimental elastic constants for DPE at 77K†

Source	c_{11}	c^L_{110}	c^T_{110}	$\bar{c}$	c_{22}	E_a	E_b
Kitagawa and Miyazawa[5]	8.1	11.9	3.2	6.6	11.4	6.7	9.4
Tasumi and Krimm[4]	15.3	19.8	6.0	12.1	20.3	13.5	17.9
Williams set IV	12.5	14.1	3.0	6.3	10.9	8.9	7.8
Williams set VII	12.4	14.0	2.9	6.3	11.1	8.8	7.9
Experimental	11.5	14.2	–	[6.5]	–	–	–

† Units 10^{10} dyne cm^{-2}

comparison can be made after scaling down the frequency to take into account the inertial change. A figure of 75 cm^{-1} (2K) may be contrasted with the value of 72 cm^{-1} (77K) observed here, which is very satisfactory considering the temperature difference. The assignment of the 111 cm^{-1} mode to the overall chain rotatory A_g mode was followed up by the authors in conjunction with Harley and Hayes[29]. Laser Raman spectroscopy of single crystal textured NPE prepared by the method described earlier revealed a completely polarized band at 136.5 cm^{-1} (77K) indicating a mode A_g symmetry. Similar experiments on DPE were hindered by fluorescence of the light brown material in the laser beam. A figure of 110 cm^{-1} (77K) can be derived for the DPE A_g mode frequency from the NPE data. This figure gives excellent agreement with the neutron data reported here. Assignment of the B_{3g} mode at 108 cm^{-1} in NPE at 77K from the Raman measurements suggests a mode at 87 cm^{-1} in DPE and compares with the singularity observed weakly at 96 cm^{-1} in the [300] zone centre scan[6]. Better neutron data are required before this discrepancy can be deemed significant. Twisleton and White[2] have assigned a peak at 98 (123) cm^{-1} in the incoherent neutron spectrum of polycrystalline DPE (NPE) to overall rotatory motion of the chains. The zone centre frequencies for in-phase and out-of-phase rotatory modes measured at 87 (108) and 110 (137) cm^{-1} of B_{3g} and A_g symmetry appear to be consistent with this assignment since density of states calculations by Kitagawa and Miyazawa[5] suggest that these two zone centre singularities occur on either side of the peak for external rotatory motion of the chains.

CONCLUSIONS

Elastic constants and moduli of polyethylene

The mosaic spread prevented a complete determination of the elastic constants of polyethylene from acoustic velocities. However, three experimental parameters determined in this work can be compared with the predictions of various models and used to select the optimum set of elastic constants from the calculations. Such a comparison was attempted in ref. 2 using the one room temperature elastic constant derived there. Apart from the pseudopotential models described earlier there are two force fields provided in the literature for the low temperature crystal structure, those of Tasumi and Krimm[4] and Kitagawa and Miyazawa[5]. Both express the interchain potential in terms of harmonic force constants between nonbonded hydrogen atoms after Urey and Bradley[30]. Interchain dispersion curves calculated on a rigid chain model from these two force fields were kindly provided by Professor D. Martin and Dr D. I. Marsh and were in good agreement with the published data of these authors.

Elastic constants for these models were derived from the acoustic velocities and those relevant to the experimental data are assembled in *Table 3*. The parameters c^L_{110} and c^T_{110} are the constants obtained from longitudinal and transverse acoustic velocities along $[\zeta\zeta 0]$ and can be expressed[6,5]

$$c^L_{110}=\frac{{d_{110}}^2}{2}\left\{\frac{c_{11}}{a^2}+\frac{c_{22}}{b^2}+\frac{c_{66}}{a^2}+\frac{c_{66}}{b^2}+\left[\left(\frac{c_{11}}{a^2}+\frac{c_{66}}{b^2}-\frac{c_{22}}{b^2}-\frac{c_{66}}{a^2}\right)^2+4\left(\frac{c_{12}+c_{66}}{a^2b^2}\right)^2\right]^{1/2}\right\} \quad (5)$$

$$c^T_{110}=\frac{{d_{110}}^2}{2}\left\{\frac{c_{11}}{a^2}+\frac{c_{22}}{b^2}+\frac{c_{66}}{a^2}+\frac{c_{66}}{b^2}-\left[\left(\frac{c_{11}}{a^2}+\frac{c_{66}}{b^2}-\frac{c_{22}}{b^2}-\frac{c_{66}}{a^2}\right)^2+4\left(\frac{c_{12}+c_{66}}{a^2b^2}\right)^2\right]^{1/2}\right\} \quad (6)$$

where d_{110} is the spacing of [110] planes in angstroms.

Comparison of the experimental elastic constants derived from the $[\zeta 00]$ and $[\zeta\zeta 0]$ data with calculated constants is straightforward as they correspond to c_{11} and c^L_{110} respectively. Since the $[0\zeta 0]$ groups are found to be a compound of $[0\zeta 0]$ *LA* and $[\zeta\zeta 0]$ *TA* phonons the derived acoustic slope will be intermediate between c_{22} and c^T_{110}. The exact nature of this synthesis is an experimental unknown since the two components are not resolved in the experimental data. However, the centres of the calculated groups (*Figure 9*) are generally midway between the two component peak centres and so a mean elastic constant

$$\bar{c}=\tfrac{1}{4}((c^T_{110})^{1/2}+(c_{22})^{1/2})^2 \quad (7)$$

can be defined from the models and used in qualitative comparisons with the experimental parameter.

From *Table 3* it is clear that the best agreement between experiment and model is obtained for the atom–atom potential calculations which reproduce the experimental constants within little more than the experimental error. It appears that the force fields of Tasumi and Krimm[4] and Kitagawa and Miyazawa[5] are too strong and too weak respectively. Moreover in supporting the potential parameter force field the experimental data are suggestive of a greater isotropy in the interchain forces than has been suggested by calculations to date as can be seen by

Table 4 Calculated and experimental parameters of the interchain force field of DPE at 77K

	Zone centre mode frequency (cm^{-1})				Elastic constant (10^{10} dyne cm^{-2})			Mean error functions (%)		
Source	B_{1u}	B_{3g}	B_{2u}	A_g	c_{11}	c_{110}^{L}	$\bar{c}$	Π_ω	Π_e	Π
Experimental	72	87	103	111	11.5	14.2	[6.5]	–	–	–
Williams set IV	75	74	97	106	12.5	14.1	6.3	7.4	2.1	5.1
Williams set VII	77	75	96	105	12.4	14.0	6.3	8.2	2.1	5.6
Kitagawa and Miyazawa[5]	66	96	87	116	8.1	11.9	6.7	9.7	8.7	9.3
Tasumi and Krimm[4]	75	109	104	143	15.3	19.8	12.1	14.8	25.1	19.2

comparing c_{11} and c_{22} and E_a and E_b in *Table 3*. Tensile elastic moduli of 9×10^{10} and 8×10^{10} dyne cm^{-2} for compression along the a and b axes are suggested compared with figures of 13.5×10^{10} and 18×10^{10} dyne cm^{-2} derived from the force field of Tasumi and Krimm.

Comparison of these figures with the interchain bulk crystal modulus of 8×10^{10} dyne cm^{-2} obtained by Buckley at 77K shows good agreement[31,32]. This figure was derived as an average elastic modulus in the basal plane and has a stronger empirical basis than earlier values[33] around 4×10^{10} dyne cm^{-2} derived from a macroscopically applied stress and microscopically derived strains without considering the role of the amorphous regions. Buckley interpreted his experimental data using the model of Takayanagi, Imada and Kajiyama[34]. This model assumes that bulk polyethylene contains alternate layers of crystal and amorphous regions which provide component strains inversely proportional to their characteristic modulus when a stress is applied. Such a 'sandwich' model was justified by Buckley on morphological grounds for his specimen which contained planar lamellae stacked along the draw direction and linked by tie molecules, which can be viewed as the amorphous regions. The agreement obtained here between the interchain moduli of the microcrystal, confirmed by neutron scattering and the bulk crystal modulus of Buckley lends impressive support to such a two phase model of polyethylene from a source quite distinct from the morphological evidence, despite earlier pessimism based on the initial elastic constant measurement[2].

Model force fields for polyethylene

We now consider the model predictions of all the experimental parameters available for the interchain potential, both elastic constants and zone centre frequencies. There are seven such parameters from neutron scattering, far infra-red, and Raman spectroscopy. The B_{2u} translatory mode frequency is taken from ref. 35 and awaits confirmation by dichroism studies and the quantity $\bar{c}$ (equation (7)) is only approximate because of the composite nature of the experimental phonon group. The full set of parameters is assembled in *Table 4* together with the predictions of the four models employed in the last section. All of the figures refer to DPE at 77K. Strictly the pseudopotential predictions are for the 'no-phonon' structure but in practice introduction of zero-point and other phonons changes lattice frequencies of molecular crystals like polyethylene very little up to 77K. It is useful to define a function representing the mean percentage deviation of calculated frequencies and elastic constants from the experimental values

$$\Pi = \frac{100}{N} \sum_{k}^{N} \frac{|p_k^c - p_k^o|}{p_k^o} \tag{8}$$

where p_k^o and p_k^o are the kth calculated and observed parameter respectively. Sums restricted to the zone centre frequencies or elastic constants only are labelled Π_ω or Π_e and the latter are constructed from acoustic velocities since they are the actual observables. Values of Π, Π_ω and Π_e are given in *Table 4* for the potential parameter and Urey–Bradley force models. The predictions of the analytical pseudopotentials are evidently much closer to the experimental situation than those of Kitagawa and Miyazawa[5] although if attention is restricted to just the zone centre frequencies both models give a good fit. The two Urey–Bradley force fields might be expected to reproduce the Brillouin-zone centre frequencies more closely than the elastic constants since they are both fitted to the experimental B_{1u} mode frequency[28]. Of these two force fields the best overall fit (9%) is obtained using that of Kitagawa and Miyazawa. The force field of Tasumi and Krimm seems too strong, calculating parameters on average 19% greater than the experimental values. By contrast the potential parameter models, which do not incorporate any dynamical information at all, nor any parameters to adjust further, reproduce the experimental data of *Table 4* with an average error of 5%.

Experimental data for the zone centre and LA phonon frequencies are assembled in *Figure 13* for [ζ00] and [$\zeta\zeta$0] polarizations, together with the phonon dispersion curves calculated from Williams set VII potential parameters.

Considering the quantity of experimental information available it is rather difficult to speculate upon the importance of the assumptions basic to the pseudopotential approach. One significant feature however is the inferior agreement with the zone centre frequencies (8%) compared to the excellent fit derived for the elastic constants (2%) by the pseudopotential models. This may be a reflection of the approximation of molecular rigidity, or possibly anharmonicity. Pawley and Cyvin[36] show that the rigidity approximation has the greatest effect upon the highest frequency external modes. Moreover, Reynolds, Kjems and White[37,38] obtain the same effect in p-dichlorobenzene where their atom–atom potential gives a reasonable reproduction of the

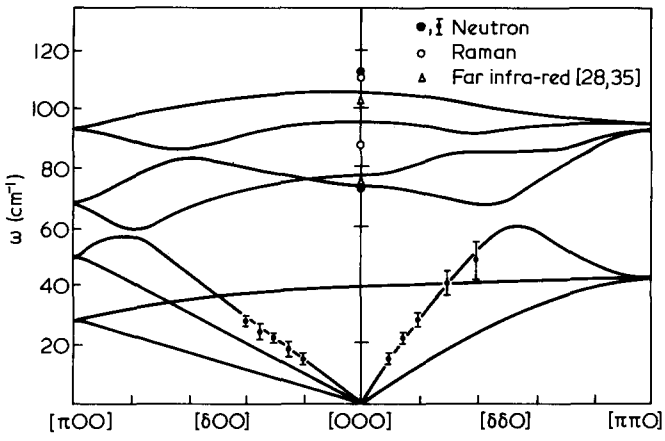

Figure 13 Phonon dispersion curves for DPE along [ξ00] and [ξξ0] calculated from Williams set VII potential parameters together with the available experimental data at 77K

experimental data for acoustic modes but is less successful for the optical branches. Even with this reservation the pseudopotential predictions are undoubtedly more substantiated by experiment than those of the Urey–Bradley force fields. Since the latter models actually rely upon some dynamical information for their construction it is especially significant that the pseudopotentials should provide the better fit, a fit that extends back from the dynamics to a whole range of structural and thermodynamic parameters.

ACKNOWLEDGEMENTS

We would like to thank Professor D. H. Martin, Drs D. I. Marsh and G. S. Pawley for providing their computer programs and Dr R. J. Young for helpful discussions about the preparation of fully oriented DPE. Dr R. W. Gray assisted in the pole figure measurements. Financial support came from the U.K. Science Research Council.

REFERENCES

1 Feldkamp, L. A., Venkataraman, G. and King, J. S. 'Neutron Inelastic Scattering', IAEA, Copenhagen, vol. 2, p. 159, 1968
2 Twisleton, J. F. and White, J. W. 'Neutron Inelastic Scattering', IAEA, Grenoble, p. 301, 1972
3 Tasumi, M. and Shimanouchi, T. *J. Chem. Phys.* 1965, **43**, 1245
4 Tasumi, M. and Krimm, S. *J. Chem. Phys.* 1967, **46**, 755
5 Kitagawa, T. and Miyazawa, T. *Jpn. Polym. J.* 1970, **1**, 471
6 Twisleton, J. F. 'Dynamical Studies of Crystalline Polymers by Inelastic Neutron Scattering', *D.Phil. thesis*, Oxford University, 1973
7 Odajima, A. and Maeda, T. *J. Polym. Sci. C* 1966, **15**, 55
8 Williams, D. E. *J. Chem. Phys.* 1966, **45**, 3770
9 *idem, ibid* 1967, **47**, 4680
10 Powell, M. J. D. *Comput. J.* 1964, **7**, 155
11 Swan, P. R. *J. Polym. Sci.* 1962, **56**, 403
12 Teare, P. W. *Acta Cryst.* 1959, **12**, 294
13 Billmeyer Jr., F. W. *J. Appl. Phys.* 1957, **28**, 1114
14 Smith, A. E. *J. Chem. Phys.* 1953, **21**, 2229
15 Shearer, H. M. and Vand, V. *Acta Cryst.* 1956, **9**, 379
16 Bunn, C. W. *Trans. Faraday Soc.* 1939, **35**, 482
17 Pawley, G. S. *Phys. Stat. Sol.* 1967, **20**, 347
18 *idem, ibid*, 1972, **49**, 475
19 Slater, J. C. 'Quantum theory of molecules and solids', vol. 2, McGraw-Hill, N.Y., 1965
20 Kitagawa, T. and Miyazawa, T. *Bull. Chem. Soc. Jpn.* 1970, **43**, 372
21 Hay, I. L. and Keller, A. *J. Mat. Sci.* 1966, **1**, 41
22 Young, R. J. 'Deformation mechanisms in crystalline polymers', *D.Phil. thesis*, Cambridge University, 1972
23 Young, R. J., Bowden, P. B., Ritchie, J. M. and Rider, J. G. *J. Mat. Sci.* 1973, **8**, 23
24 Arndt, U. W. and Willis, B. T. M. 'Single Crystal Diffractometry', Cambridge University Press, 1966
25 Baer, E. and Kardos, J. L. *J. Polym. Sci. A* 1965, **3**, 2827
26 Riste, T. in 'Instrumentation for neutron inelastic scattering research', Panel proceedings series, IAEA, Vienna, 1970
27 Brockhouse, B. N. in 'Phonons in perfect lattices and in lattices with point imperfections', (Ed. R. W. H. Stevenson), Scottish Universities Summer School, 1965
28 Krimm, S. and Bank, M. I. *J. Chem. Phys.* 1965, **42**, 4059
29 Harley, R. T., Hayes, W. and Twisleton, J. F. *J. Phys. C.* 1973, **6**, 167
30 Urey, H. C. and Bradley, C. A. *Phys. Rev.* 1930, **38**, 1969
31 Buckley, C. P. 'Creep and relaxation in isotropic and anisotropic polymeric solids', *D.Phil. thesis*, Oxford University, 1971
32 Buckley, C. P., Gray, R. W. and McCrum, N. G. *Polym. Lett.* 1969, **7**, 835
33 Sakurada, I., Ito, T. and Nakamae, K. *J. Polym. Sci. C* 1966, **15**, 75
34 Takayanagi, M., Imada, K. and Kajiyama, T. *J. Polym. Sci. C* 1966, **15**, 263
35 Dean, G. D. and Martin, D. H. *Cham. Phys. Lett.* 1967, **1**, 415
36 Pawley, G. S. and Cyvin, S. J. *J. Chem. Phys.* 1970, **52**, 4073
37 Reynolds, P. A., Kjems, J. K. and White, J. W. 'Neutron Inelastic Scattering', IAEA, Grenoble, p. 195, 1972
38 Reynolds, P. A. 'Inelastic neutron scattering from excitations in molecular crystals', *D. Phil. thesis*, Oxford University, 1972